Care and handling of mice. Both *Anxa2*$^{+/+}$ and *Anxa2*$^{-/-}$ mice were bred in ventilated shoebox cages with bedding of aspen shavings. All mice were fed with irradiated rodent diet 20 (PicoLab) and kept in a pathogen-free room equipped with Thoren ventilation, 12h/12h light/dark cycle, and constant temperature setting at 70°F. Pairs of mice were set for breeding in individual cages and adult males were removed after the pups were born.

For high oxygen treatment, P7 mouse pups together with their dam were placed in a BioSpherix ProOX A chamber equipped with ProOx P110 single setpoint oxygen controller, E702 oxygen sensor, and ProCo2 carbon dioxide sensor for 5 consecutive days (P7-P12). The ambient oxygen level was maintained at 75 ± 2%, while all other conditions, including housing, diet, cages and bedding, were the same as for the control pups maintained in room air as described above. On P12, the mice were returned to room air (21% O_2). At P17, the mouse pups were either sacrificed by CO_2 or anesthetized with avertin (0.5 mg/g body weight) for either retina isolation or intracardial perfusion, respectively. Body weights of pups were approximately 5 ± 1 g at P17. *Anxa2*$^{+/+}$ and *Anxa2*$^{-/-}$ mice exhibited no significant differences in body mass during the course of the experiments. Mouse retinas were isolated and assayed by immunoblot, RT-PCR, qRT-PCR, immunostaining, and ELISA on days 2-6 post-hyperoxia (P14-P18). Each experimental group contained 3 to 6 pups without gender preference.

Table S1. List of primers

REVERSE-TRANSCRIPTION PCR (RT-PCR)

Murine Gene	**Primer sequence**	
Anxa2	Sense	5'-CAAAATGTCTACTGTCCACGAAATC-3'
	Antisense	5'-ACCGTCATCCCCACCACACAGGTAC-3'
S100a10	Sense	5'-TCAAAATGCCATCCCAAATGG-3'
	Antisense	5'-TCGACCTATTTCTTCCCCTTCTGC-3'
Gapdh	Sense	5'-CCTTCATTGACCTCAACTAC-3'
	Antisense	5'-TCATACTTGGCAGGTTTCTC-3'
Cdh5	*Sense*	5'-GGGAATGTGCTTGCCTATGAGAG-3'
	Antisense	5'-ACGTTGATGGTGACCATGGC-3'
Hif1a	*Sense*	5'-CAAGAAACGACCGCTGCTAAGGCC-3'
	Antisense	5'-TCTCATCCATTGACTGCCCC-3'
Actb	*Sense*	5'-AGAGGGAAATCGTGCGTGAC-3'
	Antisense	5'-CAATAGTGATGACCTGGCCCGT-3'

Hif1a(exon 2) (for Hif1a$^{+/+}$ and Hif1a$^{-/-}$ MEFs genotyping)

	Sense	5'-ACTGGCTGCTATTGGGCGAAGTG-3'
	Antisense	5'-GTAAAGCACGAGGAAGCGGTCAG-3'

Human Gene	**Primer sequence**	
ANAX2	*Sense*	5'-CTCTACACCCCCAAGTGCAT-3'
	Antisense	5'-TCAGTGCTGATGCAAGTTCC-3'
ACTB	*Sense*	5'-CAAGAGATGGCCACGGCTGCT-3'
	Antisense	5'-TCCTTCTGCATCCTGTCGGCA-3'
HIF1A	*Sense*	5'-CTTCTGGATGCTGGTGATTTGG-3'
	Antisense	5'-TTTGATGGGTGAGGAATGGG-3'
S100A10	*Sense*	5'-AAATTCGCTGGGGATAAAGG-3'
	Antisense	5'-AGCCCACTTTGCCATCTCTA-3'

QUANTITATIVE REAL-TIME PCR (QRT-PCR) FOR MURINE GENES (T_m Used 60ºC)

Anxa2	*Sense*	5'-ACCAACTTCGATGCTGAGAG-3'
	Antisense	5'-GCTCCTTTTTGGTCCTTCTC-3'
S100a10	*Sense*	NA (SABiosciences, Cat. No.: PPM05269E-200)
	Antisense	NA (SABiosciences, Cat. No.: PPM05269E-200)
Hif1a	*Sense*	5'-TCTGGAAGGTATGTGGCATT-3'
	Antisense	5'-AGGGTGGGCAGAACATTTAT-3'
Actb	*Sense*	5'-AAGAGCTATGAGCTGCCTGA-3'
	Antisense	5'-TACGGATGTCAACGTCACAC-3'

Table S2. Antibodies and reagents

A. ANTIBODIES

Primary Anibodies

Antigen	Catalog No.	Isotype	Clone (if monoclonal)	Manufacturer
Actin	sc-8422	Mouse IgG	C-2	Santa Cruz
Annexin A2	Mar-00	Mouse IgG1	ZO14	Zymed
Annexin A2	610068	Mouse IgG1	5	BD Biosciences
Annexin A2 light chain (p11), human	610070	Mouse IgG1	148	BD Biosciences
Annexin A6	Sc-11388	Rabbit IgG		Santa Cruz
CD31	Ab24590	Mouse IgG1	P2B1	Abcam
CD47	sc-7057	Rabbit IgG		Santa Cruz
Fibrinogen	A008002	Rabbit IgG		DAKO
GFP	NB600-303	Rabbit IgG		Novus
HIF-1β	NB100-133	Rabbit IgG		Novus
HIF-1a, human	610958	Mouse IgG1	54	BD Biosciences
HIF-1a, mouse	NB100-105	Mouse IgG2b	H1alpha67	Novus
Isotype control	MAB002	Mouse IgG1	11711	R&D systems
Isotype control	M5534	Mouse IgG2b	MOPC-141	Sigma
p11, mouse		Rabbit IgG		Covance Research Products
Pan-Cadherin	4068S	Rabbit IgG		Cell Signaling Technology
Phospho-tyrosine (sepharose bead conjugated)	9419	Mouse IgG1		Cell Signaling Technology
Phospho-Src (Tyr 416)	2101	Rabbit IgG		Cell Signaling Technology
Phospho-VEGFR2 (Tyr 1175)	2478	Rabbit IgG		Cell Signaling Technology
Phosph-p44/42 (Thr202/Tyr204)	9101	Rabbit IgG		Cell Signaling Technology
Src	2110	Mouse IgG	L4A1	Cell Signaling Technology
VE-cadherin 5 (PE-conjugated)	560410	Mouse IgG1	55-7H1	BD Pharmingen
Vincullin	05-386	Mouse IgG1	V284	Millipore

Secondary antibodies

Antigen	Catalog No.	Conjugates	Host	Manufacturer
Mouse IgG	A21235	Alexa Fluor 647	Goat IgG	Invitrogen
Mouse IgG	AP124R	Rhodamine	Goat IgG	Millipore
Rabbit IgG	711-165-152	Cy3	Donkey IgG	Jackson Immunoresearch
Mouse IgG	NXA931	HRP	Sheep IgG	GE Healthcare
Goat IgG	Sc-2020	HRP	Donkey IgG	Santa Cruz
Rabbit IgG	NA9340	HRP	Donkey IgG	GE Healthcare

B. Other reagents

Name	Catalog No.	Manufacturer
0.5 M Tris buffer (pH 6.8)	161-0799	Biorad
1.5 M Tris buffer (pH 8.8)	161-0798	Biorad
7-amino-actinomycin D (7-AAD)	559925	BD Biosciences
Actinomycin D	A5156	Sigma
Ancrod	74/581	NIBSC
BCA protein assay reagent A	23223	Thermo Scientific
BCA protein assay reagent B	23224	Thermo Scientific
Chromatin immunoprecipitation kit	17-371	Millipore
DH5a	18265-017	Invitrogen
dNTP set (100 mM)	201912	Qiagen
Endothelial cell growth factor (100x)	E9640	Sigma
Endothelial cell growth supplement (ECGS)	E2759	Sigma
EZ-link Sulfo-NHS-SS-Biotin	21331	PIERCE
Fluoromount G	19784-25	Eletron Microscopy Sciences
H-D-Val-Leu-Lys-AMC acetate salt	I-1390	Brchem
Heparin sodium salt	H3393	Sigma
Immunopure Immobilized Strepravidin	20347	PIERCE
Isolectin B4, Fluorescein-conjugated	FL-1201	Vector Laboratories
Isolectin B4, Rhodamine-conjugated	FL-1102	Vector Laboratorites
L-glutamine	25-005-CI	Mediatech
Luciferase assay system	E4050	Promega
Mouse Fibrinogen ELISA kit	MFBGNKT	Innovative Research
Mouse lys-Plasminogen	404	American Diagnostica Inc.

M.O.M. kit for detecting mouse primary antibodies in mouse tissues	BMK-2202	Vector Laboratories
Mouse PlGF-2 ELISA kit	MP200	R & D systems
Mouse VEGF ELISA kit	MMV00	R & D systems
Nuclear Extraction Kit	78833	Thermo Scientific
One-step RT-PCR kit	210212	Qiagen
PAGEr Precast Gels (10% TBE gels)	59529	Lonza
Protease inhibitor cocktail tablet (EDTA-free)	10946900	Roche
QuantiTect Reverse Transcription kit	205311	Qiagen
Recombinant human EPO	287-TC	R & D Systems
Recombinant mouse VEGF	493-MV	R & D Systems
Slide-A-lyzer dialysis cassette	66130	PIERCE
SYBR Green PCR master mix	4309155	Applied Biosystems
TEMED (N, N, N', N'-Tetra-methylethyenediamine)	161-0801	Biorad
Trizol	15596-026	Invitrogen
Tween 20	P1379	Sigma

Figure S1. VEGF-A and placental growth factor (PlGF) are increased in mouse retinas during oxygen-induced retinopathy (OIR). (A) ELISA of VEGF-A and PlGF-2 levels in retinas collected between P12 and P18 from *Anxa2*$^{+/+}$ and *Anxa2*$^{-/-}$ mice treated with room air or hyperoxia (n = 3; **p<0.01). (B) ELISA of VEGF-A levels in different organs and tissues of *Anxa2*$^{+/+}$ and *Anxa2*$^{-/-}$ mice at P17 following room air or hyperoxia (n = 3; **p<0.01).

Figure S2. *Anxa2*$^{+/+}$ and *Anxa2*$^{-/-}$ mice maintained at room air (RA) show a similar pattern of retinal vascularization. (A) Representative images of whole-mount, isolectin B4-stained retinas collected at P17 from *Anxa2*$^{+/+}$ and *Anxa2*$^{-/-}$ mice maintained in RA. (B) Representative cross-sections (40x) and close-up views (200x) of retinal sections stained with DAPI (blue) and isolectin B4 (green). Sections were obtained at P17 from *Anxa2*$^{+/+}$ and *Anxa2*$^{-/-}$ mice maintained at RA. Scale bars, 200 µm (A), 500 µm (B, 40x), 100 µm (B, 200x). The data are representative of five independent experiments.

Figure S3. HIF-1α and p11 steady state mRNA expression, and the human A2 promoter region sequence. (A) qRT-PCR analysis of the fold change in HIF-1α mRNA levels in retinas from P12-P18 *Anxa2*$^{+/+}$ mice either maintained at room air or following 5 days of hyperoxia. (B) qRT-PCR analysis of relative p11 and HIF-1α mRNA levels in P16 retinas from Anxa2$^{-/-}$ mice either maintained at room air or following 4 days of hyperoxia (O_2). (C) A putative HIF-1α binding site (red) was identified in human A2 promoter at 378 to 373 bp upstream of the translation initiation site (green). The transcription initiation site is shown in blue. The data in A and B are representative of three independent experiments.

Figure S4. A2 mRNA stability is not affected by hypoxia. (A) RT-PCR and immunoblot (IB) analyses of HIF-1α and A2 mRNA and protein levels in HUVECs pretreated with or without

actinomycin D (10 µg/ml, 6h), followed by $CoCl_2$ (200 µM) for the indicated time periods. (B) Representative immunoblot analysis of HIF-1α and HIF-1ß expression in HEK 293 cells 24h after transfection with HIF-1α (pcDNA3.1-hif1a-CMV) and HIF-1ß (pBM5/hif1b-CMV) expression vectors. The data are representative of three independent experiments (A and B).

Figure S5. A2 deficiency does not affect HIF-1α expression. (A) Representative immunoblot (IB) and RT-PCR analyses HIF-1α and A2 in P17 retinas from both *Anxa2*$^{+/+}$ and *Anxa2*$^{-/-}$ mice maintained in room air (RA) or treated with hyperoxia (O_2). (B) Representative immunoblot and RT-PCR analyses of HIF-1α in *Anxa2*$^{+/+}$ and *Anxa2*$^{-/-}$ mouse CMECs after treatment with $CoCl_2$ (200 µM, 16h). The data are representative of three independent experiments (A and B).

Figure S6. Annexin A2 reduces fibrin deposition in mouse retinas. (A) Representative cross-sections (40x), with a higher power view of the peripheral region (200x), of P17 retinas from *Anxa2*$^{+/+}$ and *Anxa2*$^{-/-}$ mice maintained at RA. The sections were stained with DAPI (blue), isolectin B4 (green), and anti-fibrinogen (red). S, scleral side; V, vitreal side. (B) Representative immunoblot analysis of fibrin levels in P17 retinas from *Anxa2*$^{+/+}$ and *Anxa2*$^{-/-}$ mice maintained in room air (RA). Scale bars, 500 µm (A, 40x), 100 µm (A, 200x). The data are representative of five (A) or three (B) independent experiments.

Figure S7. Ancrod fails to increase retinal neo-angiogenesis in *Anxa2*$^{+/+}$ neonatal mice. (A) ELISA of fibrinogen levels (1.17 ± 0.07 vs. 0.24 ± 0.032 mg/ml; n = 6 and n = 4, respectively) in plasma of P17 post-hyperoxic *Anxa2*$^{+/+}$ mice treated with or without ancrod. (B) Representative cross-sections (40x), with higher power view of the peripheral region (200x), from P17 post-hyperoxic *Anxa2*$^{+/+}$ mice treated with or without ancrod were stained with DAPI (blue), isolectin B4 (green), and anti-fibrinogen (red). S, scleral side; V, vitreal side. (C) Representative immunoblot analysis of retinal fibrin levels in P17 post-hyperoxic *Anxa2*$^{+/+}$ mice treated with or without ancrod. (D) Representative images of retinas showing total retinal area and regions of

vaso-occlusion and neovascularization in P17 post-hyperoxic *Anxa2*$^{+/+}$ mice treated with or without ancrod. Pixel numbers for each compartment are indicated below each image. (E) Ratios of vaso-obliterative to total retinal area (22.4 ± 0.34% vs. 23.6 ± 0.99%) and neovascular to total retinal area (12.1 ± 0.86% vs. 13.5 ± 0.32%) in P17 post-hyperoxic *Anxa2*$^{+/+}$ mice treated with or without ancrod treatment (n = 4; NS, no significant difference). (F) Enumeration of neovascular nuclei in retinal sections from P17 post-hyperoxic *Anxa2*$^{+/+}$ mice treated with (208.8 ± 12.6) or without ancrod (183.5 ± 4.2) (n = 4; NS: no significant difference). Scale bars, 200 µm (B**,** 50x), 500 µm (D, 40x), 100 µm (D, 200x). The data are representative of five (B) or three (C) independent experiments.

Figure S8. Retinal neo-angiogenesis decreases in *Anxa2*$^{-/-}$ mice after treatment with tranexamic acid (TA). (A) Plasma clotting time and tPA-dependent clot lysis time for plasma samples from posthyperoxic *Anxa2*$^{-/-}$ mice after treatment with (n = 4) or without (n = 4) TA at P17. (B) Representative retinal cross-sections (4x), with close-up view of the peripheral region (200x), were stained with DAPI (blue), isolectin (green) and anti-fibrin (red) from P17 *Anxa2*$^{-/-}$ mice treated with or without TA post-hyperoxia. S, scleral side; V, vitreal side. (C) Representative immunoblot analysis of fibrin level in P17 post-hyperoxic retinas from *Anxa2*$^{-/-}$ mice treated with or without TA. (D) Images of representative retinas showing total retinal area, and regions of vaso-obliteration and neovascularization in P17 post-hyperoxic *Anxa2*$^{-/-}$ mice with or without TA treatment. Pixel number corresponding to each compartment is indicated below each image. (E) Ratios of vaso-obliterative to total retinal area (13.8 $\underline{+}$ 2.3 vs 18.5 $\underline{+}$ 2.5%) and neovascular to total retinal area (5.9 $\underline{+}$0.5 vs 3.9 $\underline{+}$ 0.2) in P17 post-hyperoxic *Anxa2*$^{+/+}$ mice treated with or without TA (n = 3). NS, no significant difference; * $p<0.05$). (F) Enumeration of neovascular nuclei in retinal sections from P17 post-hyperoxic *Anxa2*$^{-/-}$ mice treated with (68.5 $\underline{+}$ 5.5) or without (92.8 $\underline{+}$ 5.9) TA (n = 4, * $p<0.05$). Scale bars, 500 µm (B, 40x), 100 µm (B, 200x), 200 µm (D**,** 50x).The data are representative of five (B) or three (C) independent experiments.

Figure S9. Working model of retinal angiogenesis by A2 during oxygen-induced retinopathy (OIR). (A) Hypoxia stabilizes HIF-1α protein, preventing its proteasomal degradation. (B) Stabilized HIF-1α translocates into the cell nucleus, heterodimerizing with HIF-1ß. (C) HIF-1α/HIF-1ß complexes bind to the hypoxia-responsive element (HRE) within the A2 promoter, initiating transcription of A2 mRNA. (D) Newly synthesized A2 protein recruits and stabilizes p11 to form the A2 heterotetramer, which associates with the inner leaflet of the plasma membrane. (E) Hypoxia also activates Src kinase (F), which in turn phosphorylates the A2 heterotetramer at residue Tyr^{23}on A2. (G) The A2 heterotetramer translocates to the cell surface, where it binds both plasminogen (PLG) and tPA (H), stimulating the production of plasmin. (I) Plasmin degrades pericellular fibrin (J), which facilitates directed migration of vascular endothelial cells (K), promoting retinal angiogenesis. Modulation of retinal fibrin deposition by either reducing fibrinogen content (ancrod) or inhibiting plasminogen activation (TA) will influence retinal neo-angiogenesis during OIR.

Figure S1

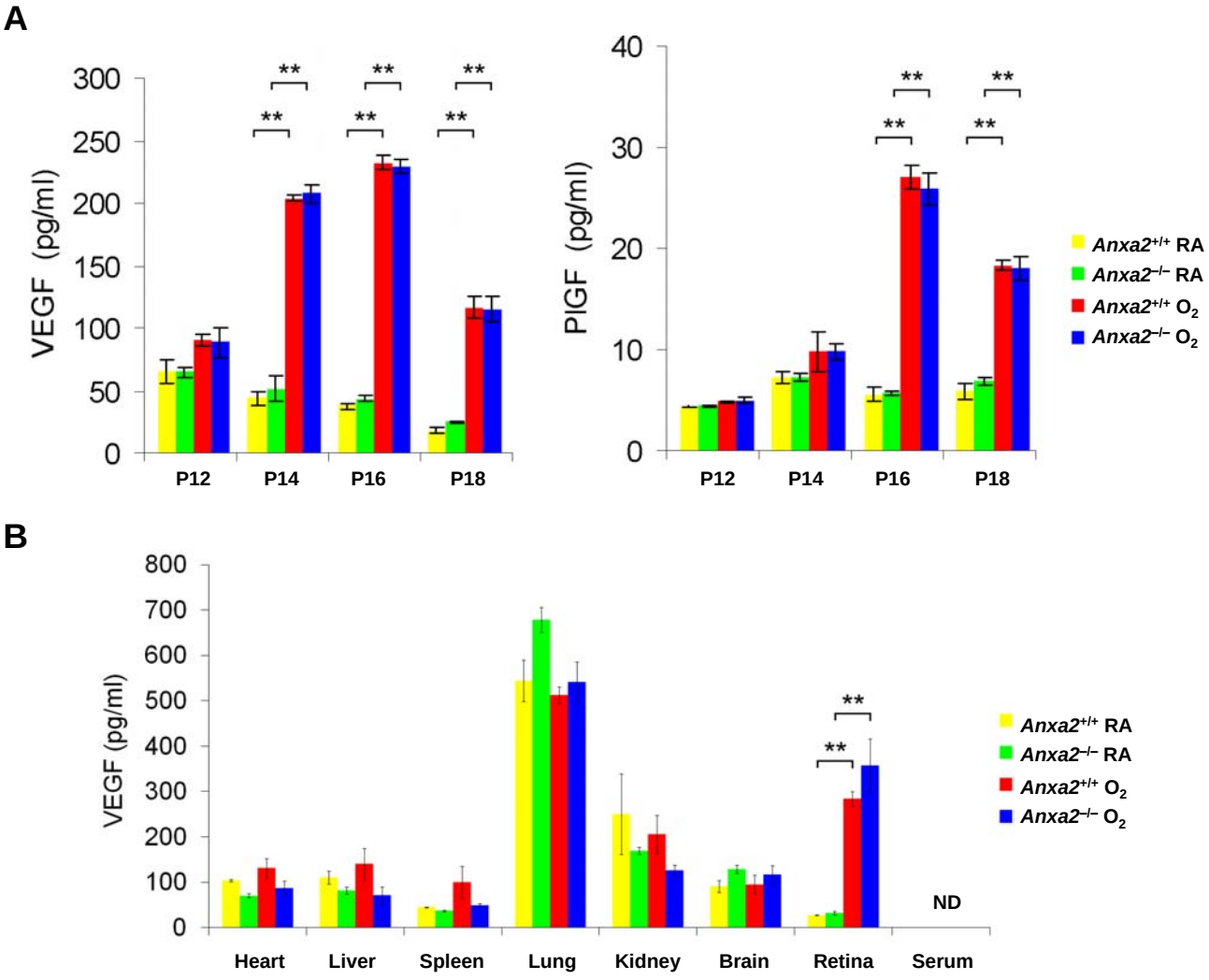
A
VEGF (pg/ml)
300
250
200
150
100
50
0
**
P12
P14
P16
P18
PIGF (pg/ml)
40
30
20
10
0
Anxa2+/+ RA
Anxa2−/− RA
Anxa2+/+ O2
Anxa2−/− O2
B
VEGF (pg/ml)
800
700
600
500
400
300
200
100
0
ND
Heart
Liver
Spleen
Lung
Kidney
Brain
Retina
Serum

Figure S2

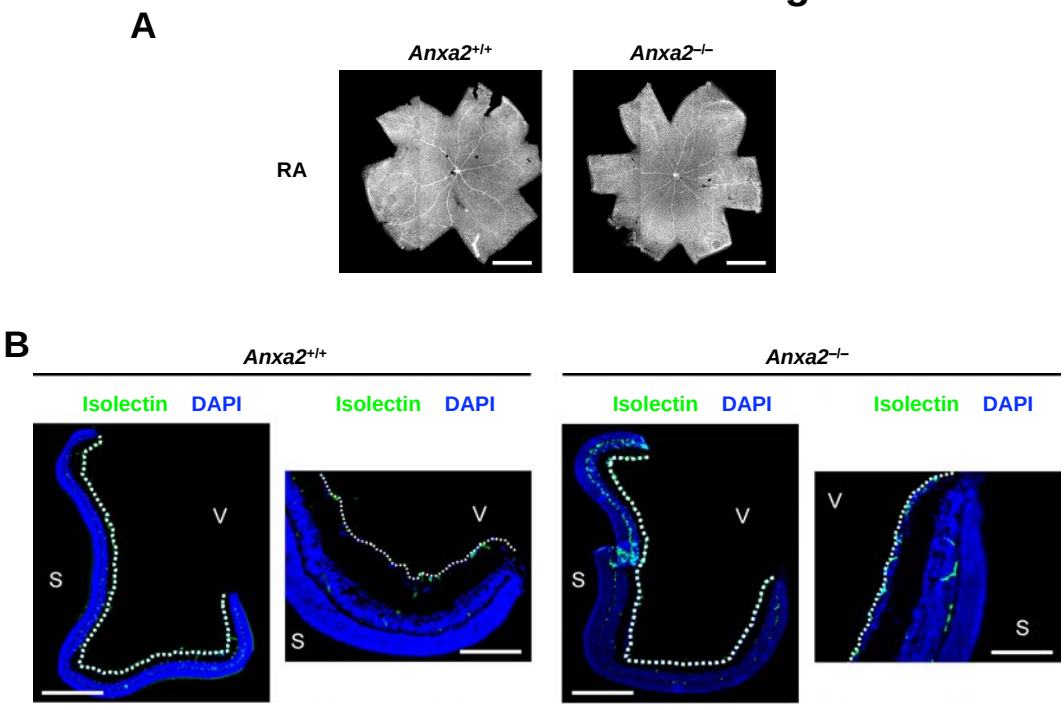
A
Anxa2+/+
Anxa2–/–
RA
B
Anxa2+/+
Anxa2–/–
Isolectin DAPI
Isolectin DAPI
Isolectin DAPI
Isolectin DAPI
V
S
V
S
V
S
V
S

Figure S3

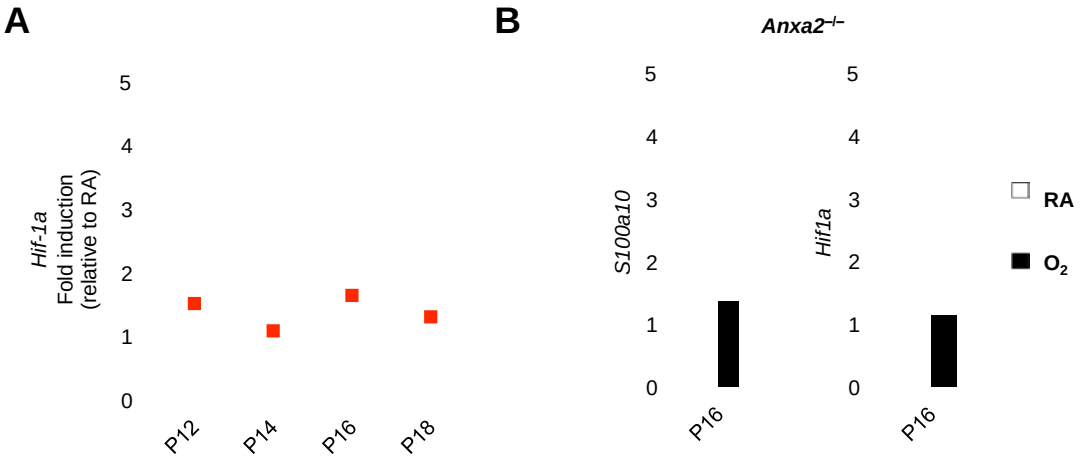

C

Human A2 promoter region

5'- CCACTTAATCAAGCCCAGAGTCTACTACTAAAGTCTTGTTAATTTATTAA

-378 -373

CCCAAGCCGAGGCTGAGAGCTC**GACGTG**GCACTTAAGAAGTAAAATGAGG

Putative HIF-1α binding site

AAAGGAGGAAGAAACGGGGTCCCTGTGGGCCTCGGGGCAGCCTCGGCCGG

GCTTTCTCGGAGGGCAGGGCCAGGGGCGCTGGGGCCGCTCCCGCGTGGCG

CGGCTCGGGAGCGTTCCAGGGCGCGGTCCCTGCGGGCCGGCGGGCCGGGG

TGAGTCACCCCTGACTTGGGGTGGGAGCGGGCCGTGTAAGGGGGAGGCGG

GGCGGGGCGGGGCGGGCCTCCCCTCGCCTAGGGAGGATGTGGCGGGTATA

-73 -68

AAAGCCCCACCCAGGCCAGCCGGCTCT**GCTCAG**CATTTGGGGACGCTCTC

Transcription initiation site

AGCTCTCGGCGCACGGCCCAGGTAAGCGGGGCGCGCCCTGCCCGCCCGCG

+1

ATGGGCCGCCAGCTAGCGG**-3'**

Translation initiation site

Figure S4

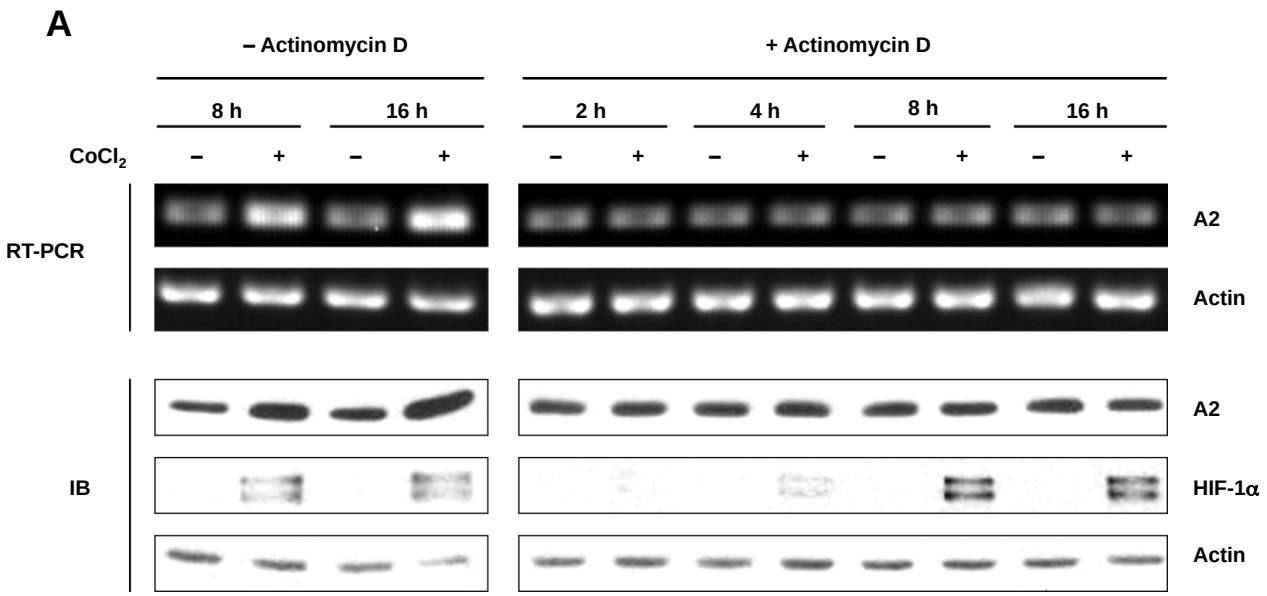
A
– Actinomycin D
+ Actinomycin D
8 h
16 h
2 h
4 h
8 h
16 h
CoCl2
– + – + – + – + – + – + – +
RT-PCR
A2
Actin
IB
A2
HIF-1α
Actin

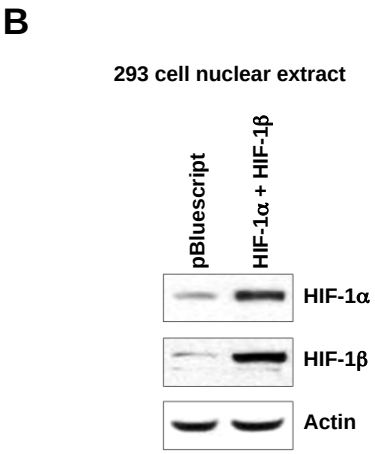
B
293 cell nuclear extract
pBluescript
HIF-1α + HIF-1β
HIF-1α
HIF-1β
Actin

Figure S5

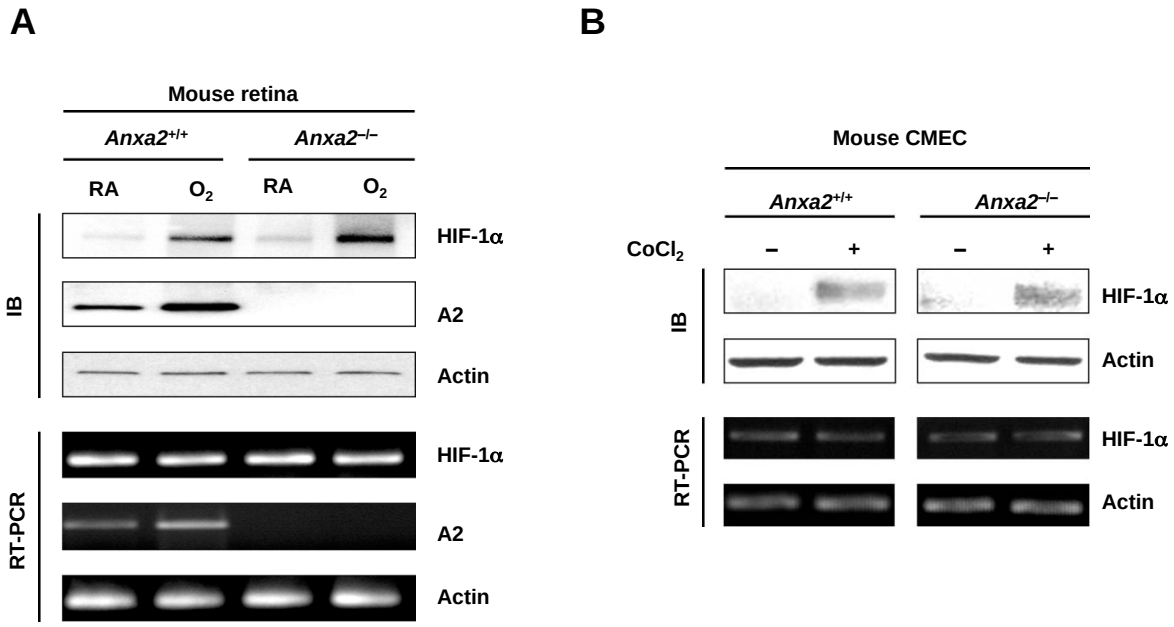
A
Mouse retina
Anxa2+/+
Anxa2–/–
RA
O2
RA
O2
IB
HIF-1α
A2
Actin
RT-PCR
HIF-1α
A2
Actin
B
Mouse CMEC
Anxa2+/+
Anxa2–/–
CoCl2
–
+
–
+
IB
HIF-1α
Actin
RT-PCR
HIF-1α
Actin

Figure S6

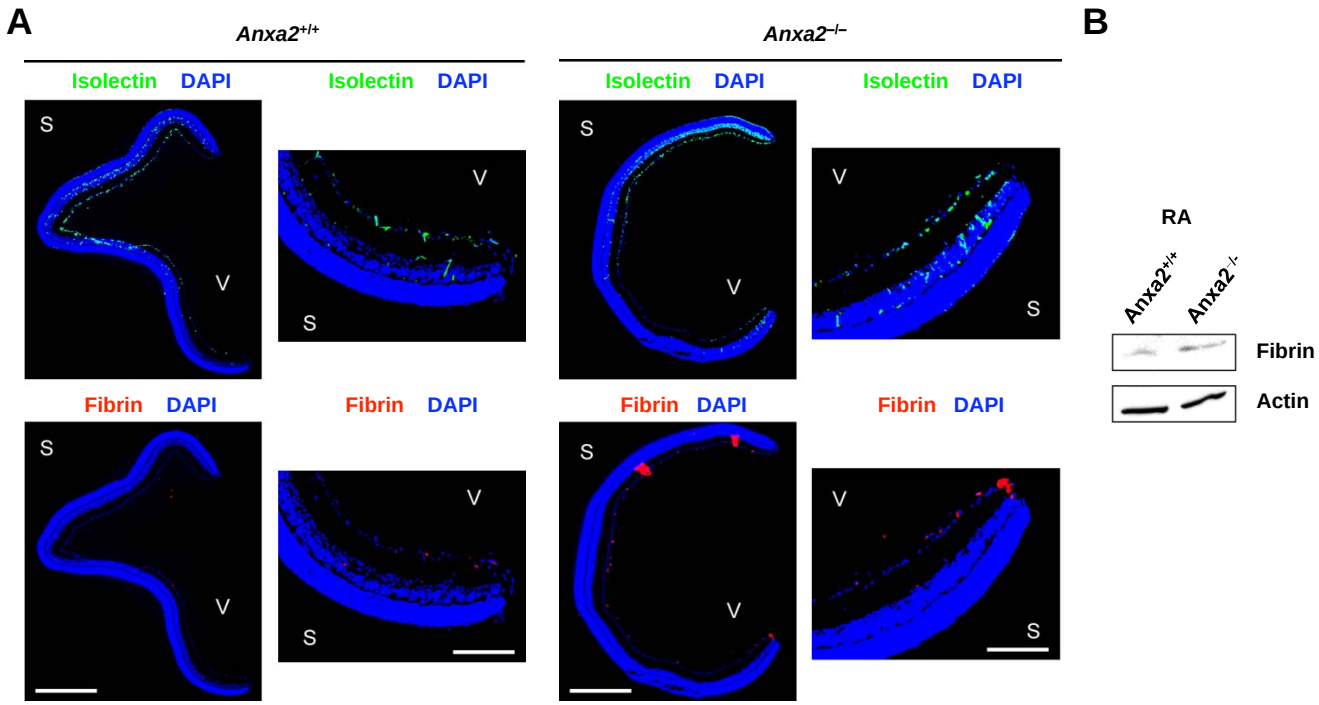
A
Anxa2+/+
Anxa2−/−
Isolectin DAPI
Isolectin DAPI
Isolectin DAPI
Isolectin DAPI
Fibrin DAPI
Fibrin DAPI
Fibrin DAPI
Fibrin DAPI
S
V
B
RA
Anxa2+/+
Anxa2−/−
Fibrin
Actin

Figure S7

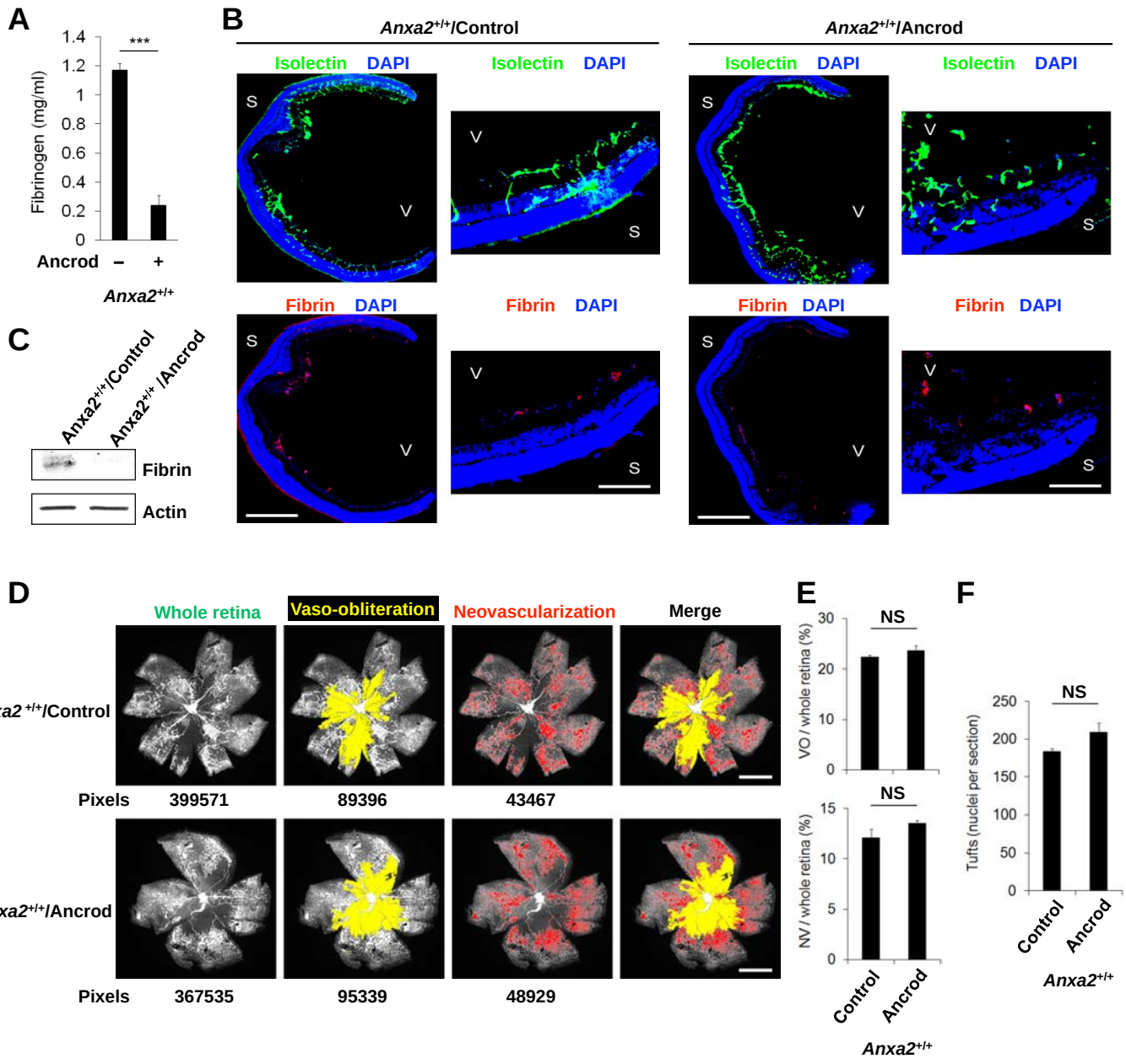
A
Fibrinogen (mg/ml)
1.4
1.2
1
0.8
0.6
0.4
0.2
0
***
Ancrod – +
Anxa2+/+
B
Anxa2+/+/Control
Anxa2+/+/Ancrod
Isolectin DAPI
Fibrin DAPI
S
V
C
Anxa2+/+/Control
Anxa2+/+ /Ancrod
Fibrin
Actin
D
Whole retina
Vaso-obliteration
Neovascularization
Merge
Anxa2 +/+/Control
Pixels 399571 89396 43467
Anxa2+/+/Ancrod
Pixels 367535 95339 48929
E
VO / whole retina (%)
NS
NV / whole retina (%)
NS
Control
Ancrod
Anxa2+/+
F
Tufts (nuclei per section)
NS
Control
Ancrod
Anxa2+/+

Figure S8

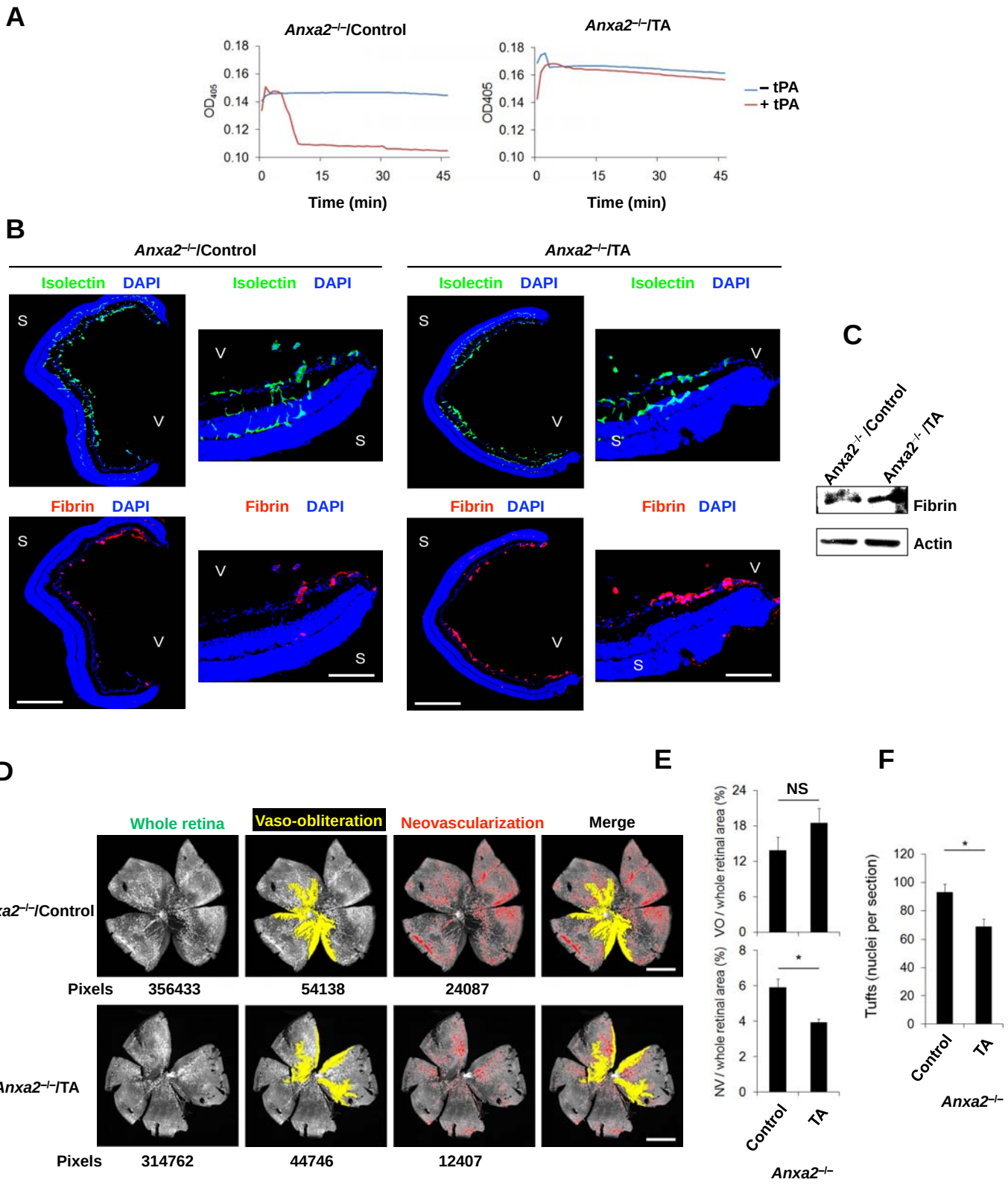
A
Anxa2−/−/Control
Anxa2−/−/TA
OD405
0.18
0.16
0.14
0.12
0.10
0
15
30
45
Time (min)
– tPA
+ tPA
B
Anxa2−/−/Control
Anxa2−/−/TA
Isolectin DAPI
Fibrin DAPI
S
V
C
Anxa2−/−/Control
Anxa2−/−/TA
Fibrin
Actin
D
Whole retina
Vaso-obliteration
Neovascularization
Merge
Anxa2−/−/Control
Pixels 356433 54138 24087
Anxa2−/−/TA
Pixels 314762 44746 12407
E
NS
VO / whole retinal area (%)
NV / whole retinal area (%)
Control
TA
Anxa2−/−
F
Tufts (nuclei per section)
Control
TA
Anxa2−/−

Figure S9

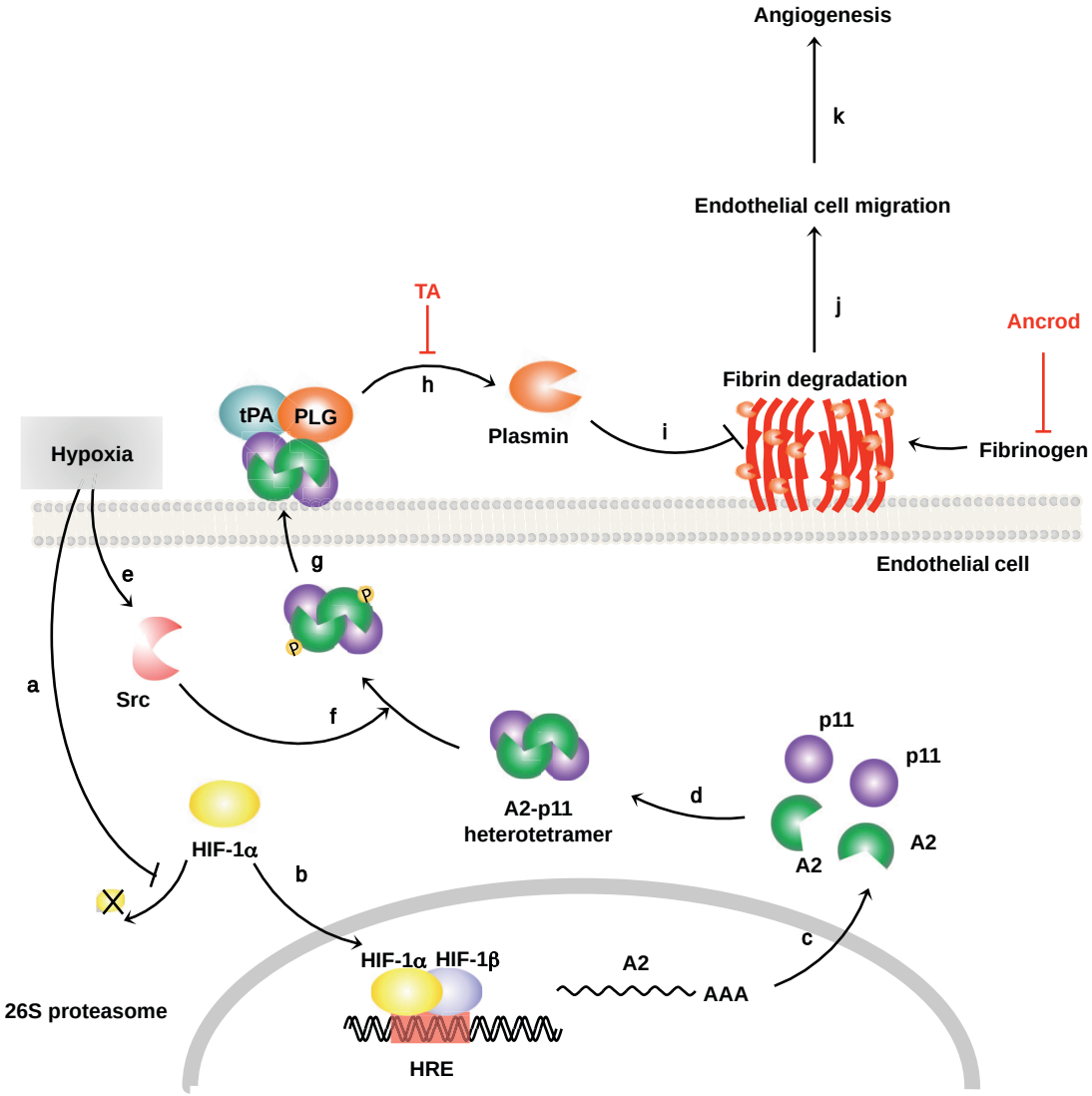
Angiogenesis
k
Endothelial cell migration
j
TA
Ancrod
h
tPA
PLG
Plasmin
i
Fibrin degradation
Fibrinogen
Hypoxia
Endothelial cell
g
e
P
P
Src
a
f
p11
p11
A2-p11
heterotetramer
d
A2
A2
HIF-1α
b
c
HIF-1α HIF-1β
A2
AAA
26S proteasome
HRE